molecular pharmaceutics

pubs.acs.org/molecularpharmaceutics

Article

Time and Temperature Dependence of Drug Crystallization—The Role of Molecular Mobility

N. S. Krishna Kumar, Rahul Lalge, and Raj Suryanarayanan*

Cite This: *Mol. Pharmaceutics* 2024, 21, 5880−5891

Read Online

ACCESS | Metrics & More | Article Recommendations | Supporting Information

ABSTRACT: Using the time−temperature−transformation diagrams, we demonstrated a correlation between molecular mobility and crystallization in amorphous solid dispersions of nifedipine (NIF) with each polyvinylpyrrolidone vinyl acetate (PVPVA64) and polyvinyl caprolactam polyvinyl acetate-polyethylene glycol graft copolymer (Soluplus). The behavior was compared with the NIF dispersions prepared with each polyvinylpyrrolidone (PVP) and hydroxypropyl methylcellulose acetate succinate (HPMCAS) [Lalge et al., *Mol. Pharmaceutics* 2023, *20*(3), 1806−1817]. Each system was characterized by a unique temperature at which the crystallization onset time was the shortest. Below this temperature, a coupling was observed between the α-relaxation time determined by dielectric spectroscopy and crystallization onset time. Above this temperature, the activation barrier for crystallization had a more significant role than molecular mobility. In the solid state, PVP and PVPVA64 dispersion exhibited higher resistance to crystallization than HPMCAS and Soluplus. The role of polymers in inhibiting crystal growth in nucleated systems was discerned by monitoring crystallization following wetting of the amorphous dispersion with the dissolution medium. PVPVA64 and Soluplus dispersions exhibited higher resistance to crystal growth than PVP and HPMCAS.

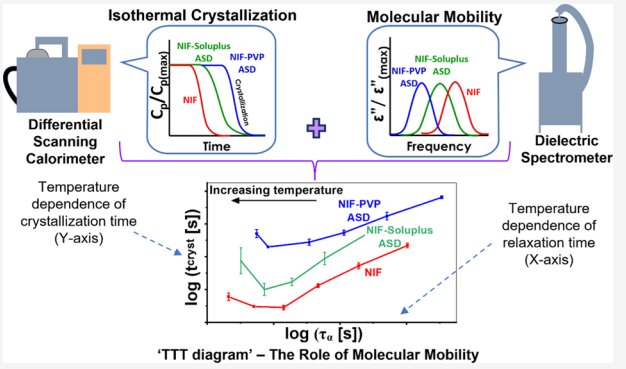

KEYWORDS: *amorphous solid dispersion, nifedipine, polyvinylpyrrolidone vinyl acetate (PVPVA64), hydroxypropyl methylcellulose acetate succinate (HPMCAS), Soluplus, nucleation, crystallization, drug-polymer interactions, time−temperature−transformation, molecular mobility, activation energy*

INTRODUCTION

Amorphization is one of the effective methods to improve the solubility of poorly water-soluble compounds.[1,2] Amorphous solid dispersions (ASDs) are a molecular mixture of a drug and polymer, wherein the amorphous drug is stabilized in a polymeric matrix. This has the potential for a significant enhancement in the stability and solubility of amorphous drugs.[3] The design, preparation, and evaluation of ASDs have been extensively discussed and reviewed in the literature.[4]

Developing an effective ASD formulation is challenging because the overall formulation performance depends on (a) retaining the drug in the amorphous state during the manufacture and shelf life of the product and (b) retaining the solubility advantage of the amorphous form *in vivo* so as that it can translate to enhanced bioavailability.[5,6] ASDs can be commercially manufactured using scalable processes such as hot-melt extrusion (HME) and spray drying.[7] In the spray-drying method, the drug and polymer are dissolved in a solvent (or a combination of solvents), followed by solvent removal through evaporation to yield an ASD.[8] Generally, a secondary drying step is necessary to remove the residual solvent during this process.[9,10] In fusion-based techniques such as HME, heat and shear forces are utilized to melt and mix drug and polymer, followed by cooling and further downstream processing. Since the HME process does not require the use of solvents, it has caught the attention of the industrial and scientific community.[4]

There have been numerous approaches toward rational polymer selection. Ideally, an ASD should be a molecular mixture of drug and polymer. It should be devoid of drug crystals and seeds (or nuclei) since the latter, under favorable conditions, can eventually grow into crystals.[11] A stronger drug−polymer interaction will translate to increased physical stability (resistance to crystallization) of amorphous drugs in ASD. A rational approach for polymer selection was developed based on the difference in solubility parameter values between the drug and polymer and the experimental determination of the miscibility.[12] While formulating ASDs, it is also crucial to consider the inherent glass-forming ability of the drug.[13]

Received: August 19, 2024
Revised: September 23, 2024
Accepted: September 24, 2024
Published: October 3, 2024

Furthermore, the amount of polymer needed to create an amorphous form of a compound correlated with the drug's inherent crystallization tendency.[14]

The solubility advantage of ASDs can be actualized by preventing drug crystallization when the dispersions come into contact with the dissolution medium. The enhancement in oral bioavailability hinges on maintaining drug supersaturation in the gastrointestinal fluid.[15−17] It has been reported that the drug-polymer systems capable of hydrogen bonding in the solution state are more effective in preventing drug crystallization, compared to combinations without such interaction.[18,19] The aqueous solubility of the polymer will impact the rate and evolution of supersaturation.[20,21] With soluble polymers, there is an initial surge in drug concentration, leading to supersaturation, followed by a sharp decline in drug concentration. When the polymer is poorly water-soluble, the drug supersaturation is built up gradually and sustained over an extended period.[21] It is also well-known that the residual drug crystallinity in ASDs affects their dissolution performance.[22,23] If there is drug nucleation in an ASD, but with no evidence of crystallization, the supersaturation could not be sustained.[24] Polymers in the dispersion can effectively suppress both nucleation and crystal growth.[25] This speaks to the need for selecting a polymer that also effectively inhibits the nucleation of a drug.

Molecular mobility is a critical factor that dictates the physical stability of amorphous drugs. In ASDs, a polymer is added to reduce the molecular mobility of the drug. It is broadly accepted that the free energy difference drives the amorphous to crystalline transition; however, molecular mobility is considered the facilitator, and the activation barrier is the modulator of the crystallization.[26,27] Systems with high molecular mobility show a strong crystallization propensity.[28,29] The general rule of thumb for an ASD to remain physically stable over an extended period is that its storage temperature must be at least 50 °C below T_g.[30]

Molecular mobility encompasses two types of motions: global and local. Global mobility, also known as α-relaxation, involves cooperative molecular movement that becomes more pronounced as the temperature approaches the T_g.[31,32] On the other hand, local motions, referred to as β-relaxation or secondary relaxation, involve non-cooperative modes that can affect either a portion or the entire molecule. Global mobility has been associated with physical instability. In many compounds, increased global mobility correlates with a higher crystallization likelihood.[33,34] Molecular mobility can be the kinetic driving force for the nucleation and growth steps in crystallization.[27] The long-range cooperative motions (also referred to as global mobility) responsible for the glass transition are often correlated to physical stability. The influence of the strength of drug-polymer interactions on the molecular mobility of ASDs was earlier demonstrated.[35,36] An increase in molecular mobility manifested as a decrease in the α-relaxation time, facilitated crystallization.[35] Numerous studies have reported a coupling relation between the crystallization time and the α-relaxation above T_g.[37−39]

The relationship between crystallization and temperature can be more comprehensively grasped through the time and temperature dependence of crystallization onset time, which is depicted in a time−temperature−transformation (TTT) diagram. The TTT diagram plots temperature (y-axis) as a function of crystallization onset time (x-axis). The TTT curve is the phase boundary between the completely amorphous phase and the region of crystal growth. At a temperature between T_g and T_m (melting point), the crystallization onset time exhibits a minimum. This typical C-shaped TTT curve is due to the net effect of the kinetic and thermodynamic driving forces for nucleation and growth. The role of molecular mobility (or viscosity) and activation barrier on TTT diagrams was shown for several amorphous drugs.[26,40,41] Each compound was characterized by a unique C-curve reflecting its physical stability. An increase, either in polymer concentration or the strength of drug-polymer interaction, will cause a shift in the TTT curve of ASDs toward a longer onset time.[42]

Amorphous to crystalline transformation occurs through nucleation followed by crystal growth. Even though nucleation does not guarantee growth, in order for crystallization to occur, nuclei must be present. Typically, the approaches toward polymer selection have focused on detecting crystallization. From a practical viewpoint, nucleation information may be much more valuable for stability prediction, as it is the precursor to crystallization. Senapati et al. constructed "nucleation rate curves" for ionic glass-forming liquids by altering nucleation times and temperatures followed by detecting crystallization. The authors identified the time required at each temperature to cause nucleation.[43] The crystal nucleation and growth rates of two indomethacin polymorphs were determined.[28] Recently, the favorable temperature ranges for the nucleation and growth of L-arabitol and ibuprofen were identified.[27,44] However, all these investigations were conducted using only the drug substance.

Nucleated ASDs can "appear" to be completely amorphous with no obvious evidence of crystallinity. These nuclei, acting as seeds, can promote rapid drug crystallization when the ASD comes in contact with the GI fluids.[24] As a result, supersaturation may not be maintained for practically useful time scales. Consequently, enhancement in bioavailability, which is the goal of the ASD formulation, may be severely compromised. To minimize the risk of drug crystallization, it is crucial to identify polymers that can inhibit drug nucleation *as well as* crystal growth.

Previously, we used a two-step approach to construct the apparent nucleation rate curve for nifedipine (NIF) ASDs prepared with each PVP and HPMCAS. TTT diagrams were constructed to discern the conditions under which there will be (i) no nucleation, (ii) nucleation but no detectable growth, and (iii) crystal growth.[45] In this context, we identified the T_{nose}^{nucl}, the critical nucleation temperature, defined as the temperature of the shortest nucleation time. We also determined the critical cooling rate to avoid nucleation based on the TTT diagrams for nucleation.[45]

While PVP was more effective in preventing nucleation and growth, the fundamental mechanistic basis for this effect was not understood. The current work explores the impact of molecular mobility and activation barriers for drug crystallization on the TTT behavior of ASDs. To develop a comprehensive understanding, we studied the effect of two additional polymers, PVPVA64 and Soluplus, on the crystallization behavior of NIF. The results were compared with earlier results of NIF ASDs prepared with PVP and HPMCAS.

We have three objectives. (i) Generate TTT diagrams to determine the critical cooling rates to avoid drug crystallization in ASDs. (ii) Study the role of molecular mobility, determined

https://doi.org/10.1021/acs.molpharmaceut.4c00935
Mol. Pharmaceutics 2024, 21, 5880−5891

by dielectric spectroscopy, and activation barrier on drug crystallization behavior in ASDs. (iii) Explore the effect of nucleation on drug crystallization when the ASDs were wetted with a dissolution medium. We compared the effects of four polymers, which differed in their strength of interaction with the drug.

MATERIALS AND METHODS

Materials. Crystalline nifedipine was obtained from Struchem (China) and used as received. Polyvinylpyrrolidone (PVP; $M_w \sim 2000$ to 3000 g/mol), polyvinylpyrrolidone vinyl acetate (PVPVA64; $M_w \sim 45\,000$ to 70 000 g/mol), and polyvinyl caprolactam polyvinyl acetate-polyethylene glycol graft copolymer (Soluplus; $M_w \sim 90\,000$ to 140 000 g/mol) were provided by BASF (New Jersey, USA). Hydroxypropyl methylcellulose acetate succinate (HPMCAS-HF; $M_w \sim 18\,000$ g/mol) was supplied by Ashland (Delaware, USA). All the solvents and other chemicals used in the study were of analytical grade.

Differential Scanning Calorimetry. A differential scanning calorimeter (DSC) equipped with a refrigerated cooling accessory was used (Q2000, TA Instruments, Delaware, USA). The instrument was calibrated with indium and sapphire. The measurements were done under a nitrogen purge at 50 mL/min. Data were analyzed using commercially available software (Universal Analysis, TA Instruments, DE, USA).

Preparation of Amorphous Materials for Isothermal Crystallization. Drug−polymer solid dispersions were prepared using a solvent evaporation technique followed by melt quenching. Physical mixtures of drug and polymer were dissolved in methanol. The solvent was then evaporated at 55 °C under reduced pressure (IKA-HB10, Werke GmbH and Co., Germany), followed by drying at room temperature for 24 h, and also under reduced pressure. Samples were then melt-quenched *in situ* in the DSC Tzero pan. About 10 mg of each sample was filled in an aluminum pan and sealed hermetically with a lid containing a pinhole. Samples were then heated to 182 °C (10 °C above the melting point of the drug), followed by rapid cooling to the temperature of the crystallization study (T^{cryst}). T^{cryst} ranged between 60 and 120 °C. During the isothermal hold, quasi-isothermal modulated DSC was used to measure the heat capacity (C_p) as a function of time. The oscillation amplitude was set to ±0.5 °C, and the period was 60 s. The first discernible decrease in C_p was considered the crystallization onset time. The change in the C_p as a function of time formed the basis for getting a measure of drug crystallization. The onset of crystallization will be evident from the time of discernible decrease in the C_p.[26]

Crystallization Onset Time for Generating TTT Diagram. The procedure for the construction of TTT diagrams was previously discussed in detail.[26,42] Crystallization onset (t^{cryst}) was the time of the first discernible decrease in the C_p value. The critical cooling rate to avoid crystallization (CR_{crit}) is the slope of the tangent to the "nose" of the phase boundary curve and is described by eq 1:[43,46]

$$CR_{crit} = \frac{T_m - T_{nose}}{t_{nose}} \tag{1}$$

where T_m is the melting temperature and T_{nose} is the temperature of the nose of the phase boundary curve and reflects the shortest crystallization time, t_{nose}.[46]

Dielectric Spectroscopy. A high-performance frequency analyzer, the Novocontrol Alpha-AK, was used to study the dielectric properties of ASDs. It was equipped with a temperature controller, the Novocool Cryosystem. The sample melt was positioned between two gold-plated copper electrodes (20 mm diameter), separated by a 0.1 mm thick silica spacer. The sample was melted on a hot plate and was quickly cooled to room temperature, yielding a film of the ASD. The isothermal dielectric measurements were conducted over a frequency range of $10^{-1} - 10^6$ Hz, while heating the sample from 40 to 120 °C in increments of 5 °C. The data were analyzed using WinFiT software, and fit parameters for the Havriliak−Negami (HN) equation were obtained:

$$\varepsilon^*(\omega) = \varepsilon_\infty + \frac{\Delta\varepsilon}{(1 + (i\omega\tau_{HN})^\alpha)^\gamma} + \frac{\sigma_0}{i\omega\varepsilon_0} \tag{2}$$

In this equation, complex dielectric permittivity, $\varepsilon^*(\omega)$, which consists of real (ε') and imaginary (ε'') components, can be obtained from the dielectric data. The ω represents the angular frequency, ε_∞ is the high-frequency dielectric constant, ε_0 is the free space permittivity, and σ_0 is the conductivity. The term $\sigma_0/i\omega\varepsilon_0$ is the conductivity contribution to dielectric data. The $\Delta\varepsilon$ is the dielectric strength of the relaxation process, and τ_{HN} is the relaxation time in the HN function. The shape parameters α and γ represent, respectively, the symmetric and asymmetric broadening of the dielectric loss. The average mobility of the system, τ_α, is taken as the relaxation time corresponding to the dielectric loss peak, and it was obtained from the following relationship.

$$\tau_\alpha = \tau_{HN}\left[\sin\left(\frac{\alpha\pi}{2 + 2\gamma}\right)\right]^{-1/\alpha}\left[\sin\left(\frac{\alpha\gamma\pi}{2 + 2\gamma}\right)\right]^{1/\alpha} \tag{3}$$

Synchrotron X-ray Diffractometry. NIF crystallization, following wetting the amorphous dispersion with the dissolution medium, was studied using synchrotron radiation. Approximately 10 mg of each ASD was weighed in a Tzero DSC pan and stored at 50 °C in an oven (to induce nucleation) for predetermined times. The samples were stored at −20 °C until analyses in the synchrotron beamline. At the beamline, 10 μL phosphate buffer saline (pH 6.8) was added to each pan and sealed hermetically. The samples were mounted on a custom-built sample holder plate and placed in the path of the X-ray beam (17-BM-B beamline; transmission mode) at the Advanced Photon Source (Argonne National Laboratory, IL, USA). The wavelength was 0.4485 Å, the beam diameter was 300 μm, and a 2-dimensional detector (XRD-1621, PerkinElmer) was used. Calibration was performed using an Al_2O_3 standard (SRM 674a, NIST). The sample was scanned 15 times, with an exposure of 1 s for each scan, while oscillating along the horizontal axis (±2 mm from the center) using a motorized stage, and the results were averaged. The diffraction data were obtained periodically, and the 2D diffraction patterns were integrated into one-dimensional scans using GSAS II software. Data were analyzed using commercially available software (*JADE* 2010, Materials Data, Inc.).

RESULTS AND DISCUSSION

Baseline Characterization. DSC was used to determine the glass transition temperatures of freshly prepared ASDs with each PVPVA64 and Soluplus (Figure S1) and the "as is"

https://doi.org/10.1021/acs.molpharmaceut.4c00935
Mol. Pharmaceutics 2024, 21, 5880−5891

polymers (Figure S2). As the polymer concentration was increased, there was a pronounced increase in T_g of NIF−PVPVA64 dispersions, while the change was minimal in Soluplus ASDs (Figure 1). The results were compared with our

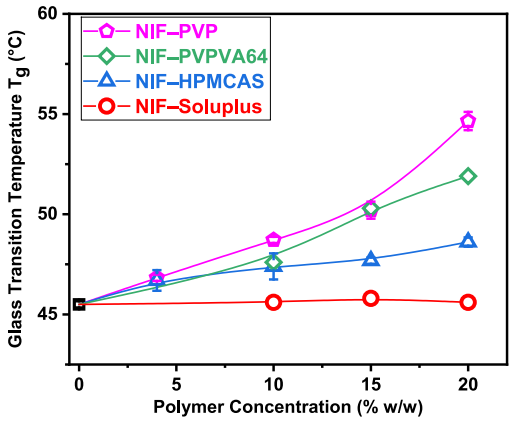

Figure 1. Plot of the glass transition temperature of ASDs as a function of polymer concentration. The error bar represents the standard deviation (n = 3).

earlier studies of NIF dispersions with PVP and HPMCAS (Figure 1). The T_g can be rank ordered as Soluplus < HPMCAS < PVPVA64 < PVP ASDs. The T_g values of PVP, PVPVA64 and HPMCAS were determined to be ∼103, 107, and 120 °C respectively (Figure S2). The pronounced effect of PVP and the more modest effect of HPMCAS on the T_g can be explained by the strength of interaction between the drug and the polymer.[35] Dielectric spectroscopy and IR spectroscopy led to the conclusion that the H-bonding of NIF with PVP was stronger than that with HPMCAS.[35] PVP is more hydrophilic than PVPVA64 and NIF solubility in PVP is greater than in PVPVA64.[47] The Flory−Huggins interaction parameter indicates that the NIF interaction with PVP is stronger than with PVPVA64.[47] However, in addition to the strength of the drug-polymer interaction, the polymer T_g is another factor that dictates the glass transition temperature.[13] The T_g of Soluplus is much lower than that of the other polymers (Figure S2), and the ASDs prepared with this polymer exhibited the lowest T_g values (Figure 1). IR spectroscopy revealed hydrogen bonding interaction between NIF and Soluplus.[48] Based on NMR, the preferred hydrogen bond interaction site of Soluplus was the vinylcaprolactam moiety.[49]

Drug Crystallization in ASDs. The film samples were prepared in the DSC, and the C_p was continuously monitored during an isothermal hold (Figure 2). The crystallization onset time was the first discernible decrease in the C_p value. As crystallization progressed, there was a gradual decrease in the observed C_p. The plots of $C_p/C_{p(max)}$ as a function of time are shown in Figure 2 for ASDs prepared with PVPVA64 (panel A) and Soluplus (panel B). A similar plot for amorphous NIF (neat drug) at 90 °C revealed an onset time (t^{cryst}) of ∼3 min.[26] The addition of polymer inhibited NIF crystallization, though the inhibitory effect was more pronounced with PVPVA64 (∼125 min at 90 °C) than with Soluplus (∼30 min; Figure 2). The effect can be attributed both to the strength of drug-polymer interaction and the polymer T_g. Our earlier studies revealed that at 15% w/w polymer concentration, PVP ASD showed a t^{cryst} of ∼460 min, while for HPMCAS ASD, it was ∼140 min.[42]

The effect of the polymer and its concentration on the NIF crystallization onset time is presented in Table 1. As the polymer concentration was increased to 20% w/w, t^{cryst} became much longer. For example, at 90 °C and with 20% w/w PVPVA64, t^{cryst} was ∼10 h, while at a slightly lower polymer concentration of 15%, t^{cryst} was ∼2 h. Furthermore, in PVPVA64 dispersions, NIF crystallized most rapidly at 110 °C, while in Soluplus dispersions, it was at 100 °C. Based on our current and earlier investigations, t^{cryst} at temperatures below 90 °C can be rank ordered as PVP > PVPVA64 > HPMCAS > Soluplus ASDs. This trend was observed for ASDs with polymer concentrations of 15% and 20% w/w.

The crystallization onset times (t^{cryst}) were utilized to construct the time−temperature−transformation (TTT) plots (Figure 3). In Figure 3, each curve represents the phase boundary between amorphous NIF (on the left of the curve) and "amorphous + crystalline" NIF (on the right of the curve). With increased polymer concentration, the curves "shift" to the right (toward longer t^{cryst}). The temperature at which t^{cryst} exhibits a minimum is referred to as T_{nose}. The t^{cryst} at T_{nose} is referred to as t_{nose}. That is the T_{nose} for PVPA and Soluplus ASDs were observed to be 110 and 100 °C, respectively. Earlier, we had observed that the T_{nose} was 90 °C for both PVP and HPMCAS ASDs.[42] The T_{nose} was the same at both 15% and 20% w/w polymer concentrations. The t_{nose} and T_{nose} from the TTT diagram enabled us to determine the critical cooling

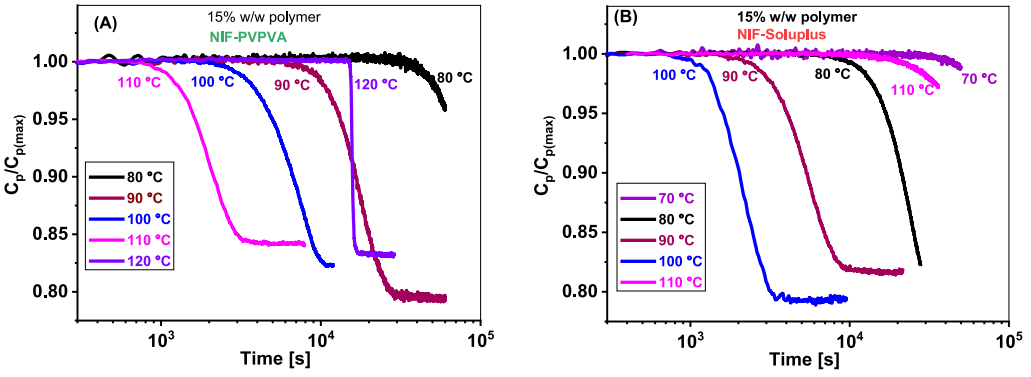

Figure 2. Plots of $C_p/C_{p(max)}$ as a function of time for (A) NIF−PVPVA64 and (B) NIF−Soluplus ASDs. The ASD was held at predetermined temperatures, and the C_p values were monitored as a function of time. $C_{p(max)}$ is the initial heat capacity value of the ASD. The polymer concentration was 15% w/w.

https://doi.org/10.1021/acs.molpharmaceut.4c00935
Mol. Pharmaceutics 2024, 21, 5880−5891

Table 1. Crystallization Onset times of NIF ASDs Prepared with Each PVPVA64 and Soluplus[a,b]

Crystallization onset time, t^{cryst} (min)								
Temp (°C)	PVPVA64 (% w/w)		Soluplus (% w/w)		HPMCAS (% w/w)		PVP (% w/w)	
	15%	20%	15%	20%	15%	20%	15%	20%
60	ND	ND	ND	ND	4000	22 000	10 700	61 100
70	2100	ND	740	ND	1040	4500	2900	9800
80	630	2000	150	630	400	1000	900	3500
90	125	600	30	200	140	370	460	1600
100	50	175	15	90	130	ND	330	ND
110	20	55	125	150	210	920	850	2600
120	130	200	ND	ND	ND	ND	ND	ND

[a]HPMCAS and PVP dispersion data were reported earlier[42] and is shown for comparison. [b]ND—not determined.

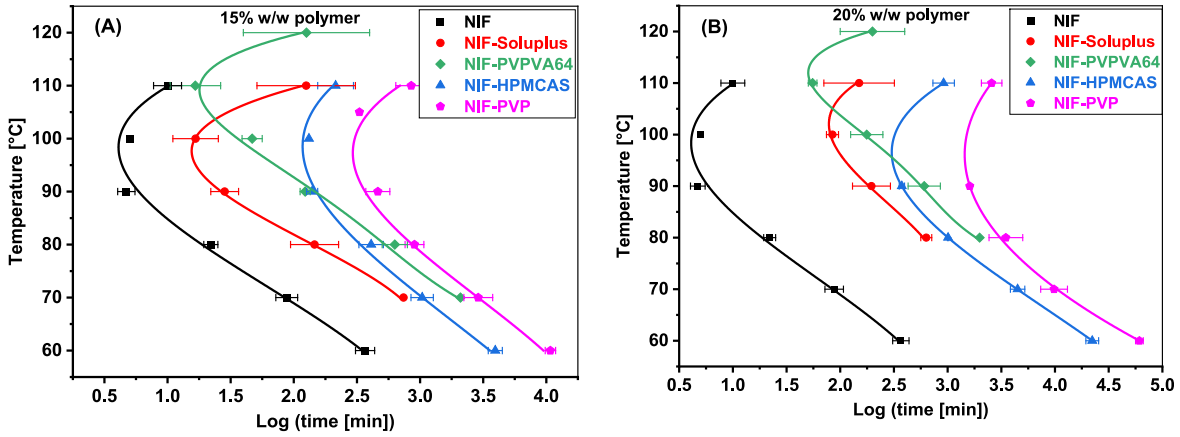

Figure 3. TTT diagrams for the crystallization onset time of NIF and NIF ASDs with polymer concentrations of (A) 15% w/w and (B) 20% w/w. Each curve represents the phase boundary between the amorphous (on the left of the curve) and "amorphous + crystalline" phases (on the right of the curve) in NIF. Crystallization data of NIF−PVP and NIF−HPMCAS ASDs obtained earlier are also included.[42]

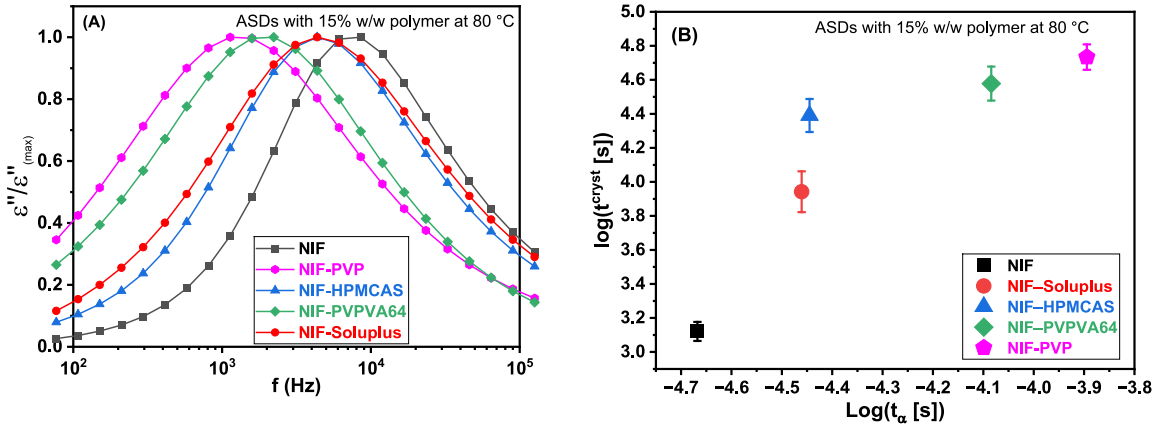

Figure 4. (A) Dielectric loss behavior of NIF and NIF ASDs at 80 °C. The loss curves have been normalized with respect to the maximum loss value. The polymer concentration was 15% w/w. (B) Crystallization time (t^{cryst}) versus α-relaxation times (τ_α) obtained from (panel A).

rate (CR_{crit}) to avoid crystallization while cooling from the melt. The CR_{crit} of ASDs with 20% w/w PVPVA64 and Soluplus were 1.1 and 0.8 °C/min, respectively. Earlier, the CR_{crit} obtained for HMPCAS and PVP ASDs (20% w/w) were 0.2 and 0.05 °C/min respectively (Figure 3B). Interestingly, in order to avoid crystallization, the NIF−PVPVA64 ASDs will need to be cooled at a slightly higher rate than the NIF−HPMCAS dispersions. However, once the dispersion is prepared, NIF−PVPVA64 ASD is more stable (longer t^{cryst}) at temperatures below 90 °C compared to HPMCAS. For example, t^{cryst} at 70 °C will be ∼1000 and 2000 min for the HPMCAS and PVPVA64 dispersions (15% w/w polymer), respectively (Figure 3A).

Role of Mobility and Activation Barrier in Drug Crystallization. The dielectric data exhibited a distinct peak attributed to α-relaxation. The dielectric loss (ε'') data was scaled with respect to the maximum loss (ε''_{max}) and the normalized data ($\varepsilon''/\varepsilon''_{max}$) was plotted as a function of frequency (Figure 4A). With a decrease in molecular mobility, the dielectric loss peak progressively shifted toward lower frequencies, reflecting longer relaxation times. At 80 °C, the relaxation peak of amorphous NIF was observed at 8×10^3 Hz

https://doi.org/10.1021/acs.molpharmaceut.4c00935
Mol. Pharmaceutics 2024, 21, 5880−5891

and is the shortest τ_α (Figure 4A). The extent of the shift in the dielectric loss peak toward the lower frequencies was unique to each polymer. While the use of HPMCAS or Soluplus resulted in a modest reduction in mobility, the effect of PVP or PVPVA64 was much more pronounced (Figure 4A). In many compounds, crystallization time and α-relaxation times (τ_α) were coupled.[37,50] The t^{cryst} were plotted against τ_α obtained from the dielectric loss peaks at 80 °C (Figure 4B). The role of mobility on the crystallization propensity of ASDs is evident in Figure 4B. An increase in τ_α results in an increase in t^{cryst}. The stability generally increases with decreased mobility, regardless of the polymer type. It is widely accepted that molecular mobility is one of the factors dictating the physical stability of amorphous systems.[27,38,39] The τ_α values of Soluplus and HPMCAS ASDs are close. However, t^{cryst} of HPMCAS dispersion is longer than that of Soluplus ASD. Interestingly, NIF−HPMCAS ASD exhibits a narrower dielectric loss peak compared to Soluplus dispersion. A broad dielectric loss indicates dynamic heterogeneity in the system.[51] To illustrate the difference in peak width, the data in Figure 4A were replotted with x-axis scaled to the frequency at dielectric loss peak (f_{max}) (Figure S3). The full width at half-maximum (fwhm) of the peak is a measure of relaxation time distribution. An ideal Debye relaxation peak, which has a single relaxation time, has a fwhm of 1.14 decades.[51] The fwhm of NIF was observed to be 1.49. With the addition of 15% HPMCAS, this was increased to 1.67 and with Soluplus, it was 1.88 (Figure S3). It is known that glass formers with broader distribution of structural relaxation times may have a reduced physical stability.[52] The crystallization behavior of ASDs indicates that, among the ASDs with similar molecular mobilities, those with narrower distribution of relaxation times have better stability. This difference in fwhm is more pronounced in 20% polymer ASDs (Figure S4A). With increase in polymer concentration, the fwhm increases while the trend is similar across different polymers. The ASDs with 20% HPMCAS and Soluplus have virtually identical τ_α. However, the HPMCAS dispersion has a higher t^{cryst} value than Soluplus ASD (Figure S4B).

The τ_α of ASDs were obtained over a temperature range of 50 to 120 °C (Figure 5). The temperature dependence of τ_α was modeled using the Vogel−Fulcher−Tammann (VFT) equation:

$$\tau_\alpha(T) = \tau_\infty \exp\left(\frac{DT_0}{T - T_0}\right) \quad (4)$$

where τ_∞ is the relaxation time of the unrestricted molecules, T_0 is the zero-mobility temperature, and D is the strength parameter. During the dielectric measurement, dispersions other than the PVP ASDs crystallized above 90 °C. However, the extrapolation of the VFT relationship enabled us to obtain the α-relaxation time up to 120 °C (Figure 5). The relaxation time of NIF ASDs can be broadly rank ordered as PVP > PVPVA64 > HPMCAS ≈ Soluplus. This trend persists in dispersions with 20% polymer (Figure S5).

A coupling between molecular mobility and crystallization propensity was established based on the assumption that the crystallization rate is a function of molecular diffusion. The drug crystallization rate G(T) can be estimated from the molecular diffusion D(T) and the thermodynamic driving force for nucleation f(T).[50]

$$G(T) = D(T)\cdot f(T) \quad (5)$$

The relationship between translational diffusion and viscosity, described by the Stokes−Einstein equation, breakdown at temperatures close to T_g. This leads to a decoupling between D(T) and τ_α:

$$D(T) \propto \frac{1}{\tau_\alpha^M(T)} \quad (6)$$

where M is the coupling coefficient. Furthermore, we can assume that G(T) is inversely related to t^{cryst}. Hence, the crystallization time is related to mobility as

$$t^{cryst}(T) \propto \frac{\tau_\alpha^M(T)}{f(T)} \quad (7)$$

This can be simplified to the following relationship:[50]

$$\log(t^{cryst}(T)) = M \log(\tau_\alpha(T)) + A(T) \quad (8)$$

where M is the coupling coefficient, and the value of A is attributed to the "influence" of thermodynamics on crystallization.

In previous studies, experiments were carried out over a limited temperature range where M was a constant.[50] However, in the current work, we are extending our experiments to a broad temperature range. At $T < T_{nose}$, the t^{cryst} values decreased as a function of τ_α. The slope of the log(t^{cryst}) versus log(τ_α) provides the coupling coefficient, M (Figure 6). In this temperature range, the value of M remains approximately constant. The M values ranged between 0.35 (for PVP) and 0.65 (for Soluplus). The value of M for the NIF and NIF ASDs can be rank-ordered as Soluplus > PVPVA64 ≈ NIF > HPMCAS ≈ PVP (Table S1). For all the systems, the M value is ≪1, reflecting that crystallization is substantially governed by factors other than mobility. We had earlier documented that, in addition to mobility, the thermodynamic activation barrier had a significant role in crystallization.[26] The resistance to crystallization increases as a function of the activation barrier. Thus, the value of A (eq 8) provides a measure of the thermodynamic barrier to crystallization. The y-intercept (A) represents the value of log(t^{cryst}) at τ_α = 1 s. The value of A for

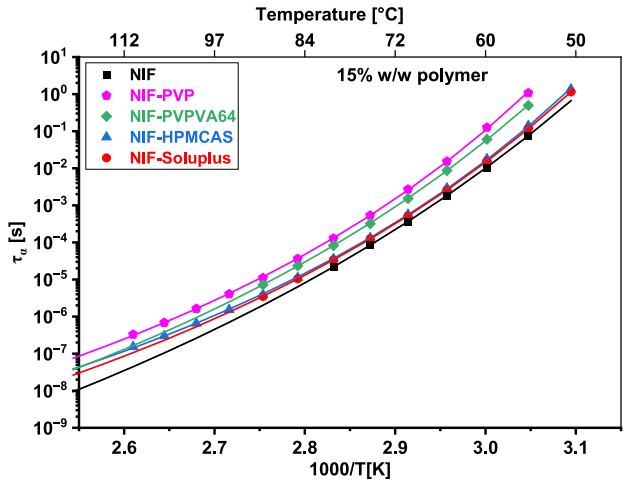

Figure 5. α-Relaxation time (τ_α) as a function of inverse temperature in NIF and NIF ASDs. The polymer concentration was 15% w/w.

https://doi.org/10.1021/acs.molpharmaceut.4c00935
Mol. Pharmaceutics 2024, 21, 5880−5891

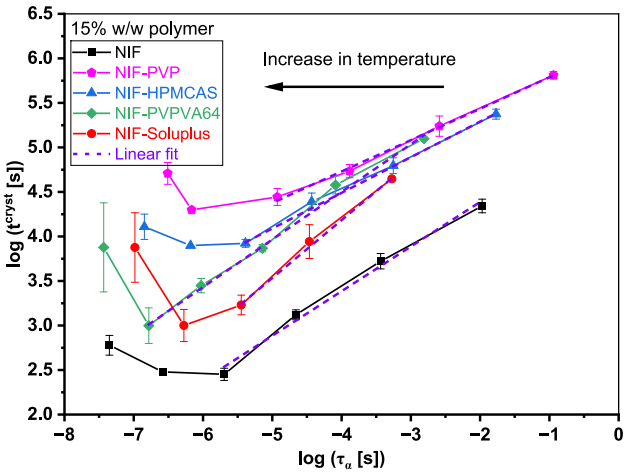

Figure 6. Relationship between the crystallization onset time, t^{cryst}, and the α-relaxation time, τ_α, of NIF ASDs (15% w/w polymer). The shortest crystallization onset time for each dispersion corresponds to the "nose" in the TTT diagram (Figure 3A).

the NIF and NIF ASDs can be rank-ordered as Soluplus ≈ PVPVA64 > PVP ≈ HPMCAS > NIF (Table S1).

However, at $T > T_{nose}$, while there was a decrease in τ_α, there was an increase in t^{cryst}. The crystallization behavior can be explained by the net effect of temperature dependencies of the molecular mobility and the activation barrier (the thermodynamic component) for crystallization. In this temperature range, while τ_α decreases as a function of temperature, the activation barrier increases. The activation energy appears to be the dominant factor influencing crystallization. The information presented in Figures 3 and 6 are complementary. Figure 3 is the classical TTT diagram, describing the effect of temperature on crystallization onset time. Figure 6 represents crystallization onset time as a function of molecular mobility. This figure shows the dependence of crystallization time on mobility at selected temperatures.

We can also explain the entire shape of the TTT diagram (Figure 3) by the net effect of the temperature dependencies of the molecular mobility and the activation barrier for crystallization. As the temperature increases, up to the nose of the TTT, molecular mobility is the limiting factor for crystallization, while, at temperatures above the nose, the activation barrier has the dominant role.

The crystallization can also be understood from a thermal activation model.[26] Herein, we consider the crystallization onset time as a function of successful jump frequency and the activation barrier associated with crystallization. The jump frequency can be related to mobility and expressed as $1/\tau_\alpha$, and E_a is the thermodynamic barrier. In this model, the relationship between crystallization time (t^{cryst}), τ_α and E_a (activation energy) is expressed as (eq 9):

$$\frac{1}{t^{cryst}(T)} = \frac{1}{N}\frac{1}{\tau_\alpha(T)}\exp\left(\frac{-E_a(T)}{RT}\right) \tag{9}$$

where N is a constant related to the number of "successful jumps" that result in crystal formation. The t^{cryst} scaled by τ_α, (t^{cryst}/τ_α), normalized the role of mobility on the crystallization propensity and described the temperature dependence of the thermodynamic barrier (Figure 7).

Furthermore, the activation barrier as a function of temperature can be obtained by rearranging eq 9 as

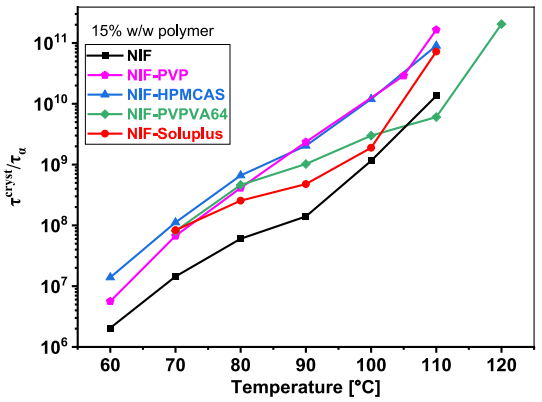

Figure 7. Plot of t^{cryst}/τ_α as a function of temperature for ASDs each with 15% w/w polymers.

$$E_a(T) = RT\ln\left(\frac{t^{cryst}(T)}{N\tau_\alpha(T)}\right) \tag{10}$$

In our earlier study, the TTT diagram of amorphous drugs was generated with the activation model, and the N value of amorphous nifedipine was determined (6.3×10^5).[26] Assuming the scaling factor N of the dispersion is the same as that of amorphous nifedipine, the activation energy barrier can be estimated as a function of temperature (Figure S6). Figures 7 and S6 are virtually identical, indicating that the t^{cryst}/τ_α as a function of temperature can be used to rank order the thermodynamic effect (activation energy) on crystallization propensity. The addition of polymer clearly results in an increase in E_a. The stability can be attributed to increased activation energy and decreased molecular mobility. For example, at 80 °C, the longer crystallization time of HPMCAS ASD compared to Soluplus ASD can be attributed to the higher activation energy of HPMCAS ASD, as both have similar relaxation times. As expected, the E_a increases with temperature for all the systems.

Effect of Nucleation. Earlier, we investigated the impact of nucleation on crystallization onset time.[45] Samples were exposed to different nucleation temperatures and their crystallization propensities were then evaluated. Compared to non-nucleated samples, the nucleated systems exhibited shorter onset times and more rapid crystallization. However, until a critical nucleation time, the crystallization onset times of the nucleated and non-nucleated samples were identical. We defined the critical nucleation time as the minimum duration to cause the nucleation density to be adequate to decrease the crystallization onset time.

The effect of nucleation on the crystallization behavior of NIF ASDs was studied. ASDs containing 20% w/w PVPVA64 or Soluplus were subjected to isothermal crystallization at 110 and 100 °C, respectively. The ASDs were first melted (at 182 °C), rapidly cooling to the selected nucleation temperature (30−70 °C), and equilibrated for ∼1 min. The samples were then heated to a crystallization temperature and held isothermally. The crystallization onset time was shorter for the nucleated samples (Figure 8). Our previous studies revealed critical nucleation times of 15 min for NIF−HPMCAS and 30 min for NIF−PVP ASDs (20% w/w polymer) at 50 °C. We, therefore, infer that the PVPVA and Soluplus systems tend to nucleate more readily than the HPMCAS and PVP ASDs.

https://doi.org/10.1021/acs.molpharmaceut.4c00935
Mol. Pharmaceutics 2024, 21, 5880−5891

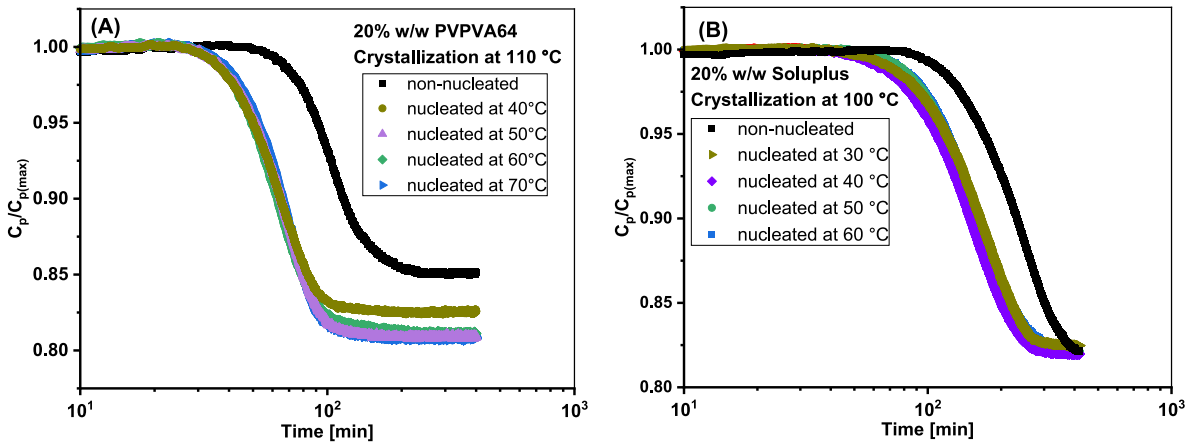

Figure 8. Isothermal crystallization behavior of NIF in dispersions. $C_p/C_{p(max)}$ as a function of time for ASDs prepared with PVPVA64 (panel A) and Soluplus (panel B). The dispersions were nucleated at different temperatures, and the crystallization kinetics was monitored at 110 °C for the PVPVA64 dispersion (panel A) and 100 °C for the Soluplus dispersion (panel B). The polymer concentration was 20% w/w.

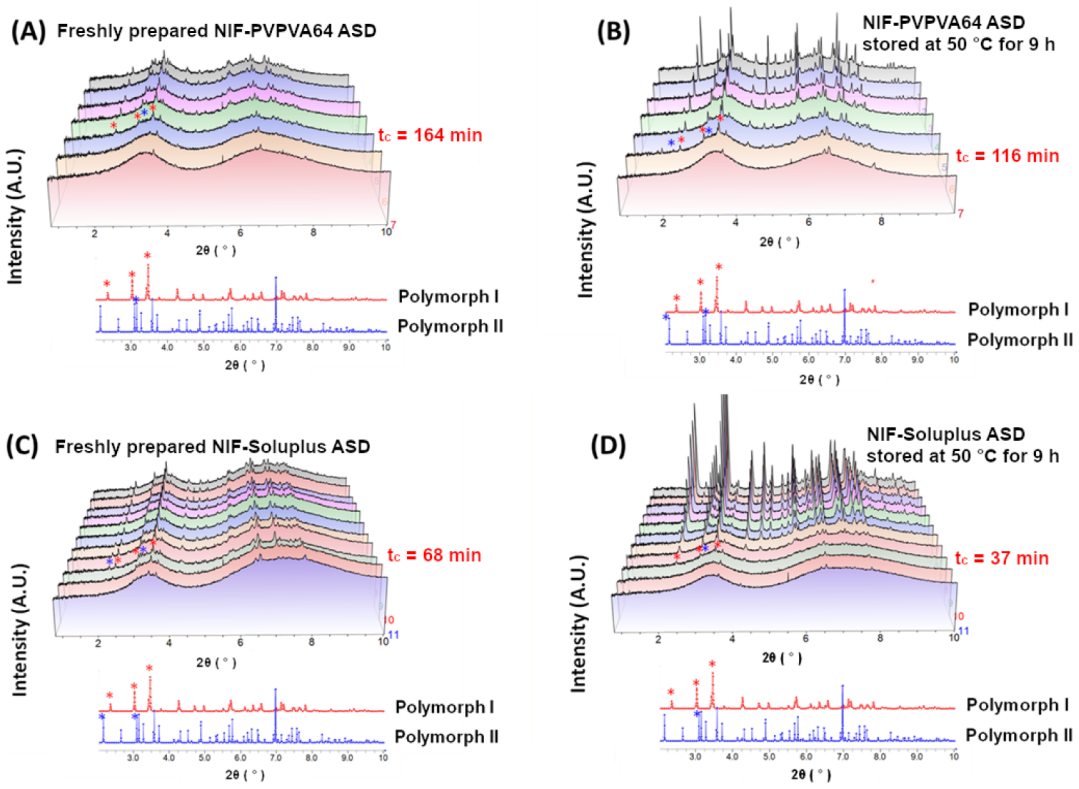

Figure 9. Overlay of XRD patterns of ASDs (20% w/w polymer) after wetting with dissolution medium (phosphate buffered saline, pH 6.8). The crystallization behavior of freshly prepared dispersions (panels A and C) is compared with nucleated dispersions (panels B and D). Only selected XRD patterns are shown. The crystallization onset time is denoted by t_c. Note that storage at 50 °C for 9 h did not result in discernible crystallization (Figure 9, panels B and D). Some characteristic peaks of NIF forms I and II are shown (Indicated by * marks).

Crystallization of ASDs in Contact with Buffer Solution. Up to this point, we have investigated the physical stability of amorphous solid dispersions (ASDs) at different temperatures. For the most part, ASDs are formulated as oral dosage forms. Following administration, the ASD will come in contact with GI fluid. In an effort to simulate the drug's *in vivo* crystallization behavior, as a simple first step, we analyzed the ASDs after wetting with phosphate buffered saline (PBS; pH 6.8). Using synchrotron radiation, the crystallization behavior of freshly prepared ASDs was determined (Figure 9). These dispersions were nucleated by storing at 50 °C for 9 h. The crystallization behavior of these wetted dispersions was also studied.

The crystallization onset time for NIF in the freshly prepared 20% w/w PVPVA64 ASD was ~164 min (Figure 9A). Nucleation decreased the lag time for NIF crystallization with the first evidence of crystallization at ~116 min (Figure 9B). In freshly prepared Soluplus ASDs (20% w/w polymer), the NIF crystallization onset time was ~68 min (Figure 9C). Following nucleation, the crystallization onset time was reduced to ~37 min (Figure 9D). The lag time in the Soluplus dispersions was shorter than that in PVPVA64

https://doi.org/10.1021/acs.molpharmaceut.4c00935
Mol. Pharmaceutics 2024, 21, 5880−5891

dispersions. Again, this could be attributed to the stronger interaction of NIF with PVPVA64. In nucleated PVP and HPMCAS ASDs, we had observed that crystallization started at ~33 and ~6 min, respectively.[45] Based on the appearance of characteristic peaks in the diffraction patterns (Figure 9), NIF usually crystallized into a mixture of forms I and II, both in freshly prepared and nucleated systems.

The influence of nucleation on the NIF crystallization behavior is summarized in Figure 10. We have compared the

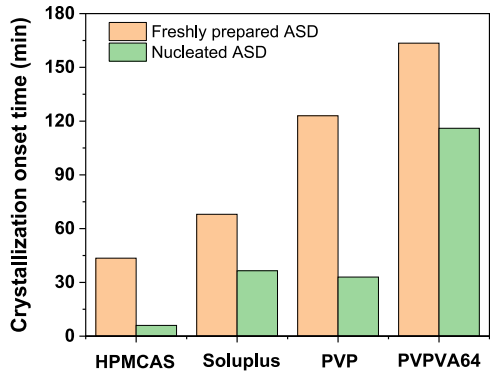

Figure 10. Comparison of the crystallization onset times after wetting with dissolution medium (phosphate buffered saline, pH 6.8) of the freshly prepared ASDs (non-nucleated) and nucleated ASDs (50 °C for 9 h). The results of the HPMCAS and PVP dispersions were reported earlier.[45]

results from our current studies with our earlier observations of HPMCAS and PVP ASDs.[45] In freshly prepared ASDs, PVPVA64 showed the longest crystallization onset time. In all the ASDs, nucleation caused a reduction in the crystallization onset time. To demonstrate the effect of each polymer on the inhibition of crystal growth in nucleated systems, the crystallization onset time of nucleated ASDs was scaled with the crystallization onset time of non-nucleated systems (Figure 11). With an increase in nucleation time, the crystallization onset time decreased. It is evident that the PVPVA64 dispersion exhibited the least detrimental effect of nucleation in the wetted systems.

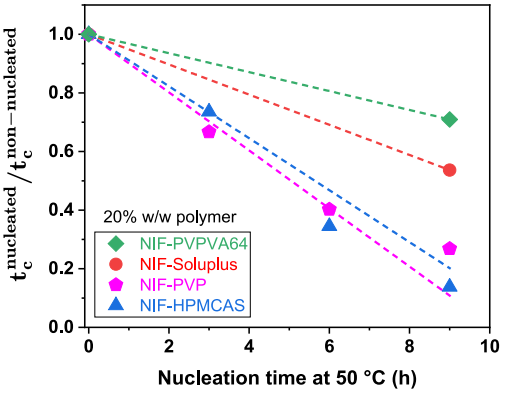

Figure 11. Scaled* crystallization onset times of nucleated ASDs prepared with each PVP, HPMCAS, PVPVA64, and Soluplus. The lines are drawn to assist in visualizing the trends. For the PVPVA64 and Soluplus dispersions, the data are presented in Figure 10, while the results of the HPMCAS and PVP dispersions were reported earlier.[45] *Scaling was done by dividing the crystallization onset of the nucleated ASD with that of the corresponding non-nucleated ASD.

SIGNIFICANCE

We have comprehensively evaluated the effect of time and temperature on the crystallization behavior of NIF in dispersions made with each PVPVA64 and Soluplus. The role of nucleation on the drug crystallization behavior was understood both in dry dispersions (i.e., in the solid state) and after wetting the dispersion with a dissolution medium. The results were compared with our earlier findings in dispersions prepared with each HPMCAS and PVP.[42,45] This enabled us to paint a comprehensive picture of the role of polymer in modulating the drug crystallization behavior under conditions that would be relevant in the manufacture, storage, and use of the formulated product.

As a first step, we identified the conditions under which the ASDs were most prone to crystallization (T_{nose}) (Figure 3). This was identified as 90, 110, 90, and 100 °C for dispersions prepared with PVP, PVPVA64, HPMCAS, and Soluplus, respectively. At temperatures < T_{nose}, crystallization was governed by molecular mobility, and resistance to crystallization in freshly prepared (non-nucleated) systems can be rank ordered as PVP > PVPVA64 > HPMCAS > Soluplus (Figure 3). However, compared to HPMCAS and PVP, both PVPVA64 and Soluplus exhibited a strong nucleation propensity (Figure 8).

When the dispersions (non-nucleated) were in contact with the dissolution medium, the resistance to crystallization can be rank ordered as PVPVA64 > PVP > Soluplus > HPMCAS (Figure 10). Following nucleation, the rank-ordering was modified to PVPVA64 > PVP ~ Soluplus > HPMCAS (Figure 10).

From the viewpoint of preparing a stable dispersion, PVP followed by PVPVA64 would be the most desirable polymers. The highest resistance to crystallization, when in contact with a dissolution medium, was exhibited by PVPVA64, followed by PVP. The superiority of PVPVA64 in resisting crystallization was retained even when the system was nucleated (Figure 10).

There is a shift in trend when comparing the crystallization propensity of freshly prepared amorphous solid dispersions (ASDs) in the solid state (dry condition) versus in a "wet" state (i.e., in contact with a buffer solution). In the solid state, the stability ranking is PVP > PVPVA64 > HPMCAS > Soluplus. However, when wetted with buffer solution, the resistance to crystallization changes to PVPVA64 > PVP > Soluplus > HPMCAS. This indicates that polymer−water interactions and polymer solubility influence the crystallization propensity of the drug. Studies have shown that rational polymer selection is essential for balancing solid-state stability and dissolution performance.[53]

The rational polymer selection requires consideration of several factors. From the perspective of solid-state stability, the molecular mobility of the system and the thermodynamic barriers to crystallization appeared to be important. When the dispersion comes in contact with the dissolution medium, identification of drug crystallization using a highly sensitive technique such as synchrotron radiation was useful. Importantly, this approach enabled us to discern the effect of nucleation on the drug crystallization kinetics. The four polymers differed widely in their ability to resist drug crystallization, both in nucleated and non-nucleated systems. Our results should be viewed with caution. The entire studies were conducted with one model drug, nifedipine. Only two polymer concentrations were studied −15 and 20% w/w. To

https://doi.org/10.1021/acs.molpharmaceut.4c00935
Mol. Pharmaceutics 2024, 21, 5880−5891

draw a broad conclusion, it will be necessary to examine the crystallization behavior of several other drugs over a wider concentration range. NIF has the potential to crystallize into different polymorphic forms. The properties of the different polymorphs are comprehensively summarized by others.[54] A detailed investigation is needed to understand the polymorphic form(s) which will crystallize in the presence of different polymers.

CONCLUSIONS

We studied the TTT diagram of NIF ASDs of four different polymers. The crystallization onset time was found to depend on both molecular mobility and activation barrier. Each exhibited a unique temperature at which the crystallization onset time was the shortest. Below this temperature, crystallization onset time is coupled to molecular mobility, while above it, the activation barrier played a significant role. We also analyzed the role of polymers in inhibiting crystal growth in nucleated systems by monitoring crystallization following wetting ASDs. We observed that PVPVA64 and Soluplus dispersions, when in contact with solution, demonstrated greater resistance to crystal growth after nucleation, compared to PVP and HPMCAS ASDs.

ASSOCIATED CONTENT

Supporting Information

The Supporting Information is available free of charge at https://pubs.acs.org/doi/10.1021/acs.molpharmaceut.4c00935.

X-ray diffraction patterns of ASDs, DSC heat follow curve showing T_g of the ASDs and polymers, scaled dielectric loss at 80 °C, τ_α of 20% polymer ASDs, and plot of E_a as a function of temperature (PDF)

AUTHOR INFORMATION

Corresponding Author

Raj Suryanarayanan − *Department of Pharmaceutics, College of Pharmacy, University of Minnesota, Minneapolis, Minnesota 55455, United States;* orcid.org/0000-0002-6322-0575; Phone: 612-624-9626; Email: surya001@umn.edu; Fax: 612-626-2125

Authors

N. S. Krishna Kumar − *Department of Pharmaceutics, College of Pharmacy, University of Minnesota, Minneapolis, Minnesota 55455, United States;* orcid.org/0000-0002-0579-9283

Rahul Lalge − *Department of Pharmaceutics, College of Pharmacy, University of Minnesota, Minneapolis, Minnesota 55455, United States;* orcid.org/0000-0001-6792-234X

Complete contact information is available at: https://pubs.acs.org/10.1021/acs.molpharmaceut.4c00935

Notes

The authors declare no competing financial interest.

ACKNOWLEDGMENTS

The project was partially supported by the William and Mildred Peters endowment fund (1701-11392-20662-UMF0003766-2108004). Parts of this work were carried out at the Characterization Facility, University of Minnesota, a member of the National Science Foundation-funded Materials Research Facilities Network (www.mrfn.org). This work used resources of the Advanced Photon Source; a U.S. Department of Energy (DOE) Office of Science User Facility operated for the DOE Office of Science by Argonne National Laboratory under Contract No. DEAC02-06CH11357. We thank Lindsay Johnson, PhD for the insightful discussions and BASF for their support (including polymer samples). We thank Dr. Andrey Yakovenko and Dr. Wenqian Xu for their help with the use of the 17BM beamline and Dr. Saul Lapidus with the use of the 11BM beamline. We thank Bhushan Munjal, PhD for proofreading the manuscript.

ABBREVIATIONS

ASD, amorphous solid dispersion(s); NIF, nifedipine; PVP, polyvinylpyrrolidone; PVPVA64, polyvinylpyrrolidone vinyl acetate; Soluplus, polyvinyl caprolactam polyvinyl acetate-polyethylene glycol graft copolymer; HPMCAS, hydroxypropyl methylcellulose acetate succinate; DSC, differential scanning calorimetry; C_p, specific heat capacity; TTT, time−temperature−transformation; t^{cryst}, crystallization onset time; T_{nose}, temperature of shortest crystallization time; t_{nose}, crystallization onset time at T_{nose} (determined by quenching the melt to the nose temperature); CR_{crit}, critical cooling rate to avoid crystallization.

REFERENCES

(1) Amidon, G. L.; Lennernäs, H.; Shah, V. P.; Crison, J. R.; Amidon, G. L.; Lennernäs, H.; Shah, V. P.; Crison, J. R. A Theoretical Basis for a Biopharmaceutic Drug Classification: The Correlation of in Vitro Drug Product Dissolution and in Vivo Bioavailability. *Pharm. Res.* **1995**, *12* (3), 413−420.

(2) Babu, N.; Nangia, A. Solubility Advantage of Amorphous Drugs and Pharmaceutical Cocrystals. *Cryst. Growth Des.* **2011**, *11*, 2662−2679.

(3) Yu, L. Amorphous Pharmaceutical Solids: Preparation, Characterization and Stabilization. *Adv. Drug Delivery Rev.* **2001**, *48*, 27−42.

(4) Huang, S.; Williams, R. Effects of the Preparation Process on the Properties of Amorphous Solid Dispersions. *AAPS PharmScitech* **2018**, *19*, 1971−1984.

(5) Bhujbal, S.; Mitra, B.; Jain, U.; Gong, Y.; Agrawal, A.; Karki, S.; Taylor, L.; Kumar, S.; Zhou, Q. Pharmaceutical Amorphous Solid Dispersion: A Review of Manufacturing Strategies. *Acta Pharm. Sin. B* **2021**, *11* (8), 2505−2536.

(6) Szabó, E.; Démuth, B.; Galata, D.; Vass, P.; Hirsch, E.; Csontos, I.; Marosi, G.; Nagy, Z. Continuous Formulation Approaches of Amorphous Solid Dispersions: Significance of Powder Flow Properties and Feeding Performance. *Pharmaceutics* **2019**, *11*, 654.

(7) Crowley, M.; Zhang, F.; Repka, M.; Thumma, S.; Upadhye, S.; Battu, S.; McGinity, J.; Martin, C. Pharmaceutical Applications of Hot-Melt Extrusion: Part I. *Drug Dev. Ind. Pharm.* **2007**, *33* (9), 909−926.

(8) Mishra, S.; Richter, M.; Mejia, L.; Sauer, A. Downstream Processing of Itraconazole: Hpmcas Amorphous Solid Dispersion: From Hot-Melt Extrudate to Tablet Using a Quality by Design Approach. *Pharmaceutics* **2022**, *14*, 1429.

(9) Démuth, B.; Nagy, Z.; Balogh, A.; Vigh, T.; Marosi, G.; Verreck, G.; Van Assche, I.; Brewster, M. Downstream Processing of Polymer-Based Amorphous Solid Dispersions to Generate Tablet Formulations. *Int. J. Pharm.* **2015**, *486*, 268−286.

(10) Kawakami, K. Current Status of Amorphous Formulation and Other Special Dosage Forms as Formulations for Early Clinical Phases. *J. Pharm. Sci.* **2009**, *98*, 2875−2885.

(11) Moseson, D.; Taylor, L. The Application of Temperature-Composition Phase Diagrams for Hot Melt Extrusion Processing of

Amorphous Solid Dispersions to Prevent Residual Crystallinity. *Int. J. Pharm.* **2018**, *553*, 454−466.
(12) Forster, A.; Hempenstall, J.; Tucker, I.; Rades, T. The Potential of Small-Scale Fusion Experiments and the Gordon-Taylor Equation to Predict the Suitability of Drug/Polymer Blends for Melt Extrusion. *Drug Dev. Ind. Pharm.* **2001**, *27* (6), 549−560.
(13) Baird, J.; Taylor, L. Evaluation of Amorphous Solid Dispersion Properties Using Thermal Analysis Techniques. *Adv. Drug Delivery Rev.* **2012**, *64*, 396−421.
(14) Van Eerdenbrugh, B.; Taylor, L. Small Scale Screening to Determine the Ability of Different Polymers to Inhibit Drug Crystallization Upon Rapid Solvent Evaporation. *Mol. Pharmaceutics* **2010**, *7*, 1328−1337.
(15) Alonzo, D. E.; Zhang, G. G. Z.; Zhou, D.; Gao, Y.; Taylor, L. S. Understanding the Behavior of Amorphous Pharmaceutical Systems during Dissolution. *Pharm. Res.* **2010**, *27* (4), 608−618.
(16) Konno, H.; Handa, T.; Alonzo, D.; Taylor, L. Effect of Polymer Type on the Dissolution Profile of Amorphous Solid Dispersions Containing Felodipine. *Eur. J. Pharm. Biopharm.* **2008**, *70*, 493−499.
(17) Newman, A.; Knipp, G.; Zografi, G. Assessing the Performance of Amorphous Solid Dispersions. *J. Pharm. Sci.* **2012**, *101*, 1355−1377.
(18) Baghel, S.; Cathcart, H.; O'Reilly, N. Theoretical and Experimental Investigation of Drug-Polymer Interaction and Miscibility and Its Impact on Drug Supersaturation in Aqueous Medium. *Eur. J. Pharm. Biopharm.* **2016**, *107*, 16−31.
(19) Chauhan, H.; Kuldipkumar, A.; Barder, T.; Medek, A.; Gu, C.; Atef, E. Correlation of Inhibitory Effects of Polymers on Indomethacin Precipitation in Solution and Amorphous Solid Crystallization Based on Molecular Interaction. *Pharm. Res.* **2014**, *31*, 500−515.
(20) Chen, Y.; Wang, S.; Wang, S.; Liu, C.; Su, C.; Hageman, M.; Hussain, M.; Haskell, R.; Stefanski, K.; Qian, F. Initial Drug Dissolution from Amorphous Solid Dispersions Controlled by Polymer Dissolution and Drug-Polymer Interaction. *Pharm. Res.* **2016**, *33*, 2445−2458.
(21) Sun, D.; Lee, P. Probing the Mechanisms of Drug Release from Amorphous Solid Dispersions in Medium-Soluble and Medium-Insoluble Carriers. *J. Controlled Release* **2015**, *211*, 85−93.
(22) Que, C.; Gao, Y.; Raina, S.; Zhang, G.; Taylor, L. Paclitaxel Crystal Seeds with Different Intrinsic Properties and Their Impact on Dissolution of Paclitaxel-Hpmcas Amorphous Solid Dispersions. *Cryst. Growth Des.* **2018**, *18*, 1548−1559.
(23) Moseson, D.; Corum, I.; Lust, A.; Altman, K.; Hiew, T.; Eren, A.; Nagy, Z.; Taylor, L. Amorphous Solid Dispersions Containing Residual Crystallinity: Competition between Dissolution and Matrix Crystallization. *Aaps J.* **2021**, *23*, 23.
(24) Yao, X.; Yu, L.; Zhang, G. Impact of Crystal Nuclei on Dissolution of Amorphous Drugs. *Mol. Pharmaceutics* **2023**, *20*, 1796−1805.
(25) Yao, X.; Huang, C.; Benson, E.; Shi, C.; Zhang, G.; Yu, L. Effect of Polymers on Crystallization in Glass-Forming Molecular Liquids: Equal Suppression of Nucleation and Growth and Master Curve for Prediction. *Cryst. Growth Des.* **2020**, *20*, 237−244.
(26) Krishna Kumar, N. S.; Suryanarayanan, R. Crystallization Propensity of Amorphous Pharmaceuticals: Kinetics and Thermodynamics. *Mol. Pharmaceutics* **2022**, *19* (2), 472−483.
(27) Descamps, M.; Dudognon, E. Crystallization from the Amorphous State: Nucleation-Growth Decoupling, Polymorphism Interplay, and the Role of Interfaces. *J. Pharm. Sci.* **2014**, *103*, 2615−2628.
(28) Andronis, V.; Zografi, G. Crystal Nucleation and Growth of Indomethacin Polymorphs from the Amorphous State. *J. Non-Cryst. Solids* **2000**, *271*, 236−248.
(29) Carpentier, L.; Desprez, S.; Descamps, M. Crystallization and Glass Properties of Pentitols - Xylitol, Adonitol, Arabitols. *J. Therm. Anal. Calorim.* **2003**, *73*, 577−586.
(30) Hancock, B.; Zograf, G. Characteristics and Significance of the Amorphous State in Pharmaceutical Systems. *J. Pharm. Sci.* **1997**, *86* (1), 1−12.
(31) Johari, G. Localized Molecular Motions of B-Relaxation and Its Energy Landscape. *J. Non-Cryst. Solids* **2002**, *307*, 317−325.
(32) Johari, G. P.; Goldstein, M. Viscous Liquids and the Glass Transition. Ii. Secondary Relaxations in Glasses of Rigid Molecules. *J. Chem. Phys.* **1970**, *53* (6), 2372−2388.
(33) Hikima, T.; Hanaya, M.; Oguni, M. Microscopic Observation of a Peculiar Crystallization in the Glass Transition Region and B-Process as Potentially Controlling the Growth Rate in Triphenylethylene. *J. Mol. Struct.* **1999**, *479*, 245−250.
(34) Kaminski, K.; Kaminska, E.; Wlodarczyk, P.; Pawlus, S.; Kimla, D.; Kasprzycka, A.; Paluch, M.; Ziolo, J.; Szeja, W.; Ngai, K. Dielectric Studies on Mobility of the Glycosidic Linkage in Seven Disaccharides. *J. Phys. Chem. B* **2008**, *112*, 12816−12823.
(35) Kothari, K.; Ragoonanan, V.; Suryanarayanan, R. The Role of Drug-Polymer Hydrogen Bonding Interactions on the Molecular Mobility and Physical Stability of Nifedipine Solid Dispersions. *Mol. Pharmaceutics* **2015**, *12* (1), 162−170.
(36) Mistry, P.; Mohapatra, S.; Gopinath, T.; Vogt, F. G.; Suryanarayanan, R. Role of the Strength of Drug-Polymer Interactions on the Molecular Mobility and Crystallization Inhibition in Ketoconazole Solid Dispersions. *Mol. Pharmaceutics* **2015**, *12* (9), 3339−3350.
(37) Bhardwaj, S. P.; Arora, K. K.; Kwong, E.; Templeton, A.; Clas, S. D.; Suryanarayanan, R. Correlation between Molecular Mobility and Physical Stability of Amorphous Itraconazole. *Mol. Pharmaceutics* **2013**, *10* (2), 694−700.
(38) Bhardwaj, S. P.; Suryanarayanan, R. Molecular Mobility as an Effective Predictor of the Physical Stability of Amorphous Trehalose. *Mol. Pharmaceutics* **2012**, *9* (11), 3209−3217.
(39) Korhonen, O.; Bhugra, C.; Pikal, M. J. Correlation between Molecular Mobility and Crystal Growth of Amorphous Phenobarbital and Phenobarbital with Polyvinylpyrrolidone and L-Proline. *J. Pharm. Sci.* **2008**, *97* (9), 3830−3841.
(40) Cheng, S.; Chakravarty, P.; Nagapudi, K.; McKenna, G. Isothermal Crystallization Monitoring and Time-Temperature-Transformation of Amorphous Gdc-0276: Differential Scanning Calorimetric and Rheological Measurements. *Mol. Pharmaceutics* **2021**, *18*, 158−173.
(41) Cheng, S.; McKenna, G. Isothermal Crystallization and Time-Temperature Transformation of Amorphous Nifedipine: A Case of Polymorphism Formation and Conversion. *Mol. Pharmaceutics* **2021**, *18*, 2786−2802.
(42) Lalge, R.; Kumar, N. S. K.; Suryanarayanan, R. Implications of Drug-Polymer Interactions on Time-Temperature-Transformation: A Tool to Assess the Crystallization Propensity in Amorphous Solid Dispersions. *Mol. Pharmaceutics* **2023**, *20* (3), 1806−1817.
(43) Senapati, H.; Kadiyala, K. K.; Angell, C. A. One- and Two-Step Calorimetric Studies of Crystallization Kinetics in Simple Ionic Glass-Forming Liquids. 1. Calcium Nitrate-Potassium Nitrate System. *J. Phys. Chem.* **1991**, *95* (18), 7050−7054.
(44) Descamps, M.; Dudognon, E.; Willart, J.-F. The Amorphous State. In *Polymorphism in the Pharmaceutical Industry*, Hilfiker, R.; Raumer, M. v., Eds.; Wiley-VCH Verlag GmbH & Co, 2018; pp. 189239. .
(45) Lalge, R.; Kumar, N. S. K.; Suryanarayanan, R. Understanding the Effect of Nucleation in Amorphous Solid Dispersions through Time-Temperature Transformation. *Mol. Pharmaceutics* **2023**, *20* (8), 4196−4209.
(46) Uhlmann, D. R. A Kinetic Treatment of Glass Formation. *J. Non-Cryst. Solids* **1972**, *7* (4), 337−348.
(47) Sun, Y.; Tao, J.; Zhang, G.; Yu, L. Solubilities of Crystalline Drugs in Polymers: An Improved Analytical Method and Comparison of Solubilities of Indomethacin and Nifedipine in Pvp, Pvp/Va, and Pvac. *J. Pharm. Sci.* **2010**, *99*, 4023−4031.
(48) Keratichewanun, S.; Yoshihashi, Y.; Sutanthavibul, N.; Terada, K.; Chatchawalsaisin, J. An Investigation of Nifedipine Miscibility in

https://doi.org/10.1021/acs.molpharmaceut.4c00935
Mol. Pharmaceutics 2024, 21, 5880−5891

Solid Dispersions Using Raman Spectroscopy. *Pharm. Res.* **2015**, *32*, 2458−2473.
(49) Sarpal, K.; Munson, E. Amorphous Solid Dispersions of Felodipine and Nifedipine with Soluplus®: Drug-Polymer Miscibility and Intermolecular Interactions. *J. Pharm. Sci.* **2021**, *110*, 1457−1469.
(50) Fung, M. H.; Suryanarayanan, R. Use of a Plasticizer for Physical Stability Prediction of Amorphous Solid Dispersions. *Cryst. Growth Des.* **2017**, *17* (8), 4315−4325.
(51) Wang, L.; Richert, R. Primary and Secondary Relaxation Time Dispersions in Fragile Supercooled Liquids. *Phys. Rev. B* **2007**, *76*, 064201.
(52) Tombari, E.; Ferrari, C.; Johari, G.; Shanker, R. Calorimetric Relaxation in Pharmaceutical Molecular Glasses and Its Utility in Understanding Their Stability against Crystallization. *J. Phys. Chem. B* **2008**, *112*, 10806−10814.
(53) Hiew, T.; Zemlyanov, D.; Taylor, L. Balancing Solid-State Stability and Dissolution Performance of Lumefantrine Amorphous Solid Dispersions: The Role of Polymer Choice and Drug-Polymer Interactions. *Mol. Pharmaceutics* **2022**, *19*, 392−413.
(54) Gui, Y.; Huang, C.; Shi, C.; Stelzer, T.; Zhang, G.; Yu, L. Polymorphic Selectivity in Crystal Nucleation. *J. Chem. Phys.* **2022**, *156*, 144504.

https://doi.org/10.1021/acs.molpharmaceut.4c00935
Mol. Pharmaceutics 2024, 21, 5880−5891